Influence of local air pollution on the deposition of peroxyacetyl nitrate to a nutrient-poor natural grassland ecosystem

A. Moravek[1*], P. Stella[1], T. Foken[2,3] and I. Trebs[1***]**

[1] Max Planck Institute for Chemistry, Biogeochemistry Department, P. O. Box 3060, 55020 Mainz, Germany

[2] Department of Micrometeorology, University of Bayreuth, Universitätsstr. 30, 95447 Bayreuth, Germany

[3] Member of Bayreuth Center of Ecology and Environmental Research (BayCEER), University of Bayreuth, Germany

* now at: Department of Chemistry, University of Toronto, 80 St. George St, ON, M5S 3H6 Toronto, Canada

** now at: AgroParisTech, UMR INRA/AgroParisTech SAD-APT, Paris, France

*** now at: Centre de Recherche Public - Gabriel Lippmann, Department Environment and Agro-Biotechnologies, 41 rue du Brill, L-4422 Belvaux, Luxembourg

Correspondence to: A. Moravek (a.moravek@utoronto.ca)

Abstract

Dry deposition of peroxyacetyl nitrate (PAN) is known to have a phytotoxic impact on plants under photochemical smog conditions, but it may also lead to higher productivity and threaten species richness of vulnerable ecosystems in remote regions. However, underlying mechanisms or controlling factors for PAN deposition are not well understood and studies on dry deposition of PAN are limited. In this study, we investigate the impact of PAN deposition on a nutrient-poor natural grassland ecosystem situated at the edge of an urban and industrialized region in Germany. PAN mixing ratios were measured within a 3.5 months summer to early autumn period. In addition, PAN fluxes were determined with the modified

Bowen ratio technique for a selected period. The evaluation of both stomatal and non-stomatal deposition pathways was used to model PAN deposition over the entire summer-autumn period. We found that air masses at the site were influenced by two contrasting pollution regimes, which lead to median diurnal PAN mixing ratios ranging between 50 and 300 ppt during unpolluted and between 200 and 600 ppt during polluted episodes. The measured PAN fluxes showed a clear diurnal cycle with maximal deposition fluxes of ~ -0.1 nmol m^{-2} s^{-1} (corresponding to a deposition velocity of 0.3 cm s^{-1}) during daytime and a significant non-stomatal contribution was found. The ratio of PAN to ozone deposition velocities was found to be ~0.1, which is much larger than assumed by current deposition models. The modelled PAN flux over the entire period revealed that PAN deposition over an entire day was 333 µg m^{-2} d^{-1} under unpolluted and 518 µg m^{-2} d^{-1} under polluted episodes. Besides, thermochemical decomposition PAN deposition accounted for 32% under unpolluted episodes and 22% under polluted episodes of the total atmospheric PAN loss. However, the impact of PAN deposition as a nitrogen source to the nutrient-poor grassland was estimated to be only minor, under both unpolluted and polluted episodes.

1 Introduction

Originating from both anthropogenic and natural sources, peroxyacetyl nitrate ($CH_3C(O)O_2NO_2$, PAN) is primarily known as an atmospheric pollutant. Both, the peroxyacetyl radical ($CH_3C(O)O_2$, PA) and nitrogen dioxide (NO_2), which form PAN via

$$CH_3C(O)O_2 + NO_2 + M \overset{k_1}{\leftrightarrow} CH_3C(O)O_2NO_2 + M \quad \text{(R1)}$$

have anthropogenic sources. Due to its thermal instability via the back reaction of R1 and subsequent reaction of PA with nitric oxide (NO),

$$CH_3C(O)O_2 + NO \overset{k_2}{\rightarrow} CH_3C(O)O + NO_2 \quad \text{(R2)}$$

long range transport of PAN in cold layers of the upper troposphere may constitute a significant source of reactive nitrogen (N_r = sum of oxidized and reduced nitrogen in remote regions. Consequently, it affects e.g. the production of ozone (O_3) and links the atmospheric and biospheric nitrogen cycle through dry deposition (Singh, 1987). Besides, locally produced PAN may also impact on ecosystems downwind of pollution sources. While high PAN mixing ratios (> 15 ppb), prevailing under strong photochemical smog conditions, PAN is known to be phytotoxic and may harm plant tissues significantly (Temple and Taylor, 1983),

the impact of PAN deposition under less extreme conditions and for lower PAN mixing ratios is not yet clear. As a nitrogen source, PAN deposition may also lead to higher productivity and may threaten species richness especially in vulnerable ecosystems (Stevens et al., 2010).

Previous studies on the surface-atmosphere exchange of PAN showed that PAN is deposited to vegetation. On the one hand, chamber experiments on PAN uptake on both leaf and plant level (Okano et al., 1990; Sparks et al., 2003; Teklemariam and Sparks, 2004) found a direct relationship between PAN uptake and stomatal conductance. They suggest that stomatal uptake is the major pathway of PAN into leaves. On the other hand, previous studies have also shown the existence of non-stomatal deposition of PAN, mainly associated with the uptake by the leaf cuticles (Teklemariam and Sparks, 2004; Turnipseed et al., 2006; Wolfe et al., 2009). While Turnipseed et al. (2006) found almost 50% of the daytime deposition to be non-stomatal for a pine forest and suggest it to be the primary deposition pathway in the upper canopy, Wolfe et al. (2009) attribute between 21 and 35% (for warm and cold periods, respectively) of the deposition flux to non-stomatal pathways for a pine forest site. However, conclusive studies on PAN fluxes are currently very limited and the obtained results differ considerably. The underlying mechanisms or controlling factors for PAN deposition, like the role of wet surfaces, as well as the relation of PAN to O_3 deposition fluxes are not well understood.

Grassland ecosystems are the third largest land use type in Europe and constitute 41% of global terrestrial surfaces (EUROSTAT, 2011; Suttie et al., 2005). Moreover, nutrient-poor habitats, where additional nitrogen input via deposition may play a significant role, are often dominated by grass species rather than trees. In this case study, we investigate the influence of polluted and non-polluted air masses on the dry deposition of PAN at a nutrient-poor natural grassland ecosystem in Central Europe. PAN mixing ratios were measured and analysed over a three months period under two contrasting pollution regimes. For a selected period, we also derived PAN fluxes with the flux-gradient approach, employing a newly developed flux measurements system for PAN (Moravek et al., 2014). In addition, fluxes of O_3, which has similarities to PAN in terms of its formation and deposition and thus is important for model applications, were determined by eddy covariance. Based on our approaches, we estimate the contribution of stomatal and non-stomatal deposition pathways for PAN and compare these results to those obtained for O_3.

2 Methods

2.1 Site description

The study was conducted at a nutrient-poor natural grassland ecosystem on the estate of the Mainz-Finthen Airport in Rhineland-Palatinate, Germany (49.9685°N, 8.1481°E). The natural grassland area of the measurement site extends over an area of 0.7 x 2.0 km (in mainly east western direction), providing good fetch condition for micrometeorological flux measurements. The ecosystem is primarily unmanaged and the vegetation is characterized by the false oat-grass (*Arrhenatherion elatioris*) plant community on dry and sandy soil with a considerable amount of senescent or died-off grass. Small bushes were occasionally removed and parts of the grassland were grazed by sheep once a year. The soil nitrate content was very low (~0.7 mg kg^{-1} in the upper 5 cm) and, hence, ammonium was most likely the largest source of plant available nitrogen from soil (~20 mg kg^{-1} in the upper 5 cm) (Oswald et al., 2013). The mean canopy height during the field campaign was 0.6 m and the bulk LAI for both green and brown grass was on average 4.8. A roughness length (z_0) of 0.1 m and a zero plane displacement (d) of 0.45 m were estimated using the approach of De Bruin and Moore (1985) for canopies with increased roughness. The site is topographically located on a plateau 150 m above the Rhine valley and located about 9 km south-west of the city centre of Mainz (Fig. 1). The plateau is part of region Rhenish Hesse, which extends to the south and south west and is characterized by agricultural land use (mainly vineyards, orchards and crops) and smaller villages. In contrast, the industrialized and densely populated Rhine-Main-Area extends to northerly and easterly directions. Two motorways bypass closely to the north and east of the site in a distance of 2 and 4 km, respectively.

2.2 Measurements of PAN mixing ratios and fluxes

PAN mixing ratios on the site were measured for a 3.5 months period in summer and early autumn 2011 (29 June to 21 October 2011) using a gas chromatograph with electron capture detection (GC-ECD, see Moravek et al. (2014) for detailed description). The GC-ECD was placed in an air-conditioned container and regularly calibrated with air from a photolytic calibration source.

In addition, during the period from 19 August to 4 September we performed gradient measurements at 0.8 and 4.0 m a.g.l. to determine biosphere-atmosphere exchanges fluxes via

the modified Bowen ratio (MBR) technique (Businger, 1986). The PAN flux ($F_{MBR_{PAN}}$) was estimated by the ratio of the PAN and O_3 mixing ratio difference between the upper and lower measurement height, Δc_{PAN} and Δc_{O3}, multiplied by the eddy covariance flux of O_3 ($F_{EC_{O3}}$):

$$F_{MBR_{PAN}} = F_{EC_{O3}} \cdot \frac{\Delta c_{PAN}}{\Delta c_{O3}} \approx F_{EC_{O3}} \cdot \frac{\Delta \chi_{PAN}}{\Delta \chi_{O3}} \quad (1)$$

We used O_3 as a proxy scalar due to its similarity to PAN in the sink and source distribution. On the one hand, the production of both PAN and O_3 is linked to photochemical processes and, on the other hand, both compounds are known to deposit to vegetation. Instead of using concentration differences in Eq. (1), we used the mixing ratio differences of PAN ($\Delta \chi_{PAN}$) and O_3 ($\Delta \chi_{O3}$) since the differences in the molar air density between the two heights were negligible. The correction of PAN fluxes for the loss by thermochemical decomposition of PAN is presented in Sect. 2.5. The storage term (see e.g., Rummel et al. (2007)) of PAN was estimated using a logarithmically interpolated vertical profile of PAN and was found to be negligible. Further details on the flux measurements, including necessary modifications of the GC-ECD and the inlet system, and an extensive error analysis are given in Moravek et al. (2014). Flux values with random errors larger than 100% were regarded as below the flux detection limit. Furthermore, under conditions with low friction velocities (u_* < 0.07 m s^{-1}) the application of the MBR methods is prone to larger errors (Liu and Foken, 2001).

2.3 Additional measurements

For the determination of O_3 eddy covariance fluxes, required for the application of the MBR method, a closed-path fast response O_3 detector (Enviscope GmbH, Germany) was employed together with a sonic anemometer (CSAT3, Campbell Scientific Inc., USA) at z_{ref} = 3 m a.g.l. (see Moravek et al. (2014) for details on eddy covariance set up and O_3 calibration). In addition, CO_2 and latent heat fluxes were determined with an open-path CO_2/H_2O analyser (LI-7500A, LI-COR, USA). All turbulent fluxes were calculated using the eddy covariance software TK3.1 (Mauder and Foken, 2011), applying state-of-the-art corrections methods as listed in Foken et al. (2012). Additionally, the O_3 flux was corrected for high frequency loss of the 2.5 m long inlet tube (Moravek et al., 2013), for the storage effect and for chemical production from NO_2 photolysis and loss by reaction with NO (Rummel et al., 2007). The nighttime removal pathway of O_3 via the reaction with NO_2 forming NO_3 (see e.g., Brown and Stutz, 2012) was found to be insignificant as the reaction

rate is about one order of magnitude lower than of the reaction of O_3 with NO. The quality scheme of Foken and Wichura (1996) was used to exclude periods with significant non-stationarity or poor developed turbulence. Data for which the footprint area of the flux measurement (calculated with a Lagrangian forward stochastic model from Rannik et al., 2000) included less than 80% of the natural grassland area were omitted.

The mixing ratio difference of O_3 between 4.0 and 0.8 m a.g.l. was determined using a differential UV absorption O_3 analyser (49i, Thermo Environmental, USA, modified according to Cazorla and Brune (2010); see Moravek et al. (2014) for details on operation). Absolute O_3 mixing ratios at both heights were derived from a vertical profiles system, which also measured NO and NO_2 mixing ratios (O_3 analyser: 49i, Thermo Environmental, USA; NO/NO_2 analyser: CLD 780 TR, Eco-Physics, Switzerland). A vertical profile of temperature, humidity and wind speed was retrieved at 0.2, 0.8, 1.5, 2.5 and 4.0 m a.g.l..

Meteorological parameters used in this study are global radiation (CNR1, Kipp&Zonen, Netherlands), NO_2 photolysis frequency (j_{NO_2}) (Meteorology Consult GmbH, Germany), rainfall (AGR100, Environmental Measurements) and surface wetness (Campbell Scientific Inc., USA). All additional measurements were performed during the entire experiment period from 29 June to 21 October 2011.

2.4 Flux partitioning

As PAN and O_3 are depositing the PAN and O_3 flux can be partitioned into deposition to leaf stomata (F_s) and to non-stomatal surfaces (F_{ns}):

$$F = F_s + F_{ns} \tag{2}$$

Following the big leaf multiple resistance approach (Hicks et al., 1987; Wesely and Hicks, 2000) the overall canopy conductance (g_c, a combination of the stomatal (g_s), the mesophyll (g_m) and the non-stomatal (g_{ns}) conductance) was obtained for both PAN and O_3 from the measured deposition velocity (v_D, i.e. the flux normalized by the concentration at z_{ref}) and the estimated aerodynamic (R_a) and quasi-laminar boundary layer (R_b) resistances (see Garland (1977) and Hicks et al. (1987), respectively):

$$g_c = \frac{1}{\frac{1}{g_s} + \frac{1}{g_m}} + g_{ns} = \left(\frac{1}{v_D} - R_a - R_b\right)^{-1} \tag{3}$$

In case processes in the leaf mesophyll (or surrounding components) do not limit the trace gas exchange (i.e. $1/g_m \sim 0$), as in the case of water vapour or O_3, g_c simply equals the sum of g_s and g_{ns}. For the calculation of the PAN stomatal uptake, no limitation of PAN uptake by the mesophyll was assumed as a first approach (see Sect. 3.3.2 for discussion on g_m). Following e.g., Lamaud et al. (2009) and Stella et al. (2011), $g_{s_{PAN}}$ and $g_{s_{O3}}$ were derived from the stomatal conductance for water vapour via the Penman-Monteith equation ($g_{s_{PM}}$) corrected for the ratio of their molecular diffusivities to the molecular diffusivity of water vapour. Due to its longer molecular structure, the diffusivity of PAN is lower ($D_{PAN} \sim 0.87 \cdot 10^{-5}$ m^2 s^{-1}) than for O_3 ($D_{O_3} \sim 1.40 \cdot 10^{-5}$ m^2 s^{-1}), which results in $g_{s_{PAN}}/g_{s_{O3}} = 0.62$ (derived from Hicks et al., 1987). Since the measured H_2O flux, on which Penman-Monteith equation is based, originated not only from transpiration through the plant stomata but also from water evaporation from other sources such as soil pores or liquid water on different surfaces, we only used dry conditions with relative humidities (RH) < 60 % to compute $g_{s_{PM}}$. Under these conditions liquid water on surfaces is assumed to be fully evaporated. Soil evaporation was excluded from $g_{s_{PM}}$ according to Stella et al. (2011). The final $g_{s_{PM}}$ values for the entire relative humidity range were determined as a function of the corrected $g_{s_{PM}}$ values against the gross primary production (GPP).

Finally, g_{ns}, representing all non-stomatal deposition pathways, e.g., to leaf cuticles, soil or water surfaces, was derived by the difference between g_c and g_s (Eq. (3)).

The findings on $g_{ns_{PAN}}$ from the partitioning of $F_{MBR_{PAN}}$ were used to model PAN deposition fluxes for the entire period from 29 June to 21 October. Applying the resistive scheme given in Eq. (3), the modelled PAN flux ($F_{model_{PAN}}$) was derived as

$$F_{model_{PAN}} = -\left(R_a + R_{b_{PAN}} + \frac{1}{g_{s_{PAN}} + g_{ns_{PAN}}}\right)^{-1} \cdot \rho_m \cdot \chi_{PAN} \quad (4)$$

where R_a,, $R_{b_{PAN}}$ and $g_{s_{PAN}}$ were determined as described above over the entire period. Here, ρ_m and χ_{PAN} represent the molar air density and the PAN mixing ratio, respectively, at the height of the eddy covariance measurements (z_{ref})

2.5 Determination of PAN loss by thermochemical decomposition

Next to dry deposition process, other sink terms impact the measured surface PAN mixing ratios. While PAN photolysis and reaction with the hydroxyl radical (OH) are expected to be

very low at altitudes below 7 km (Talukdar et al., 1995), thermochemical decomposition of PAN (back reaction of R1) has to be considered. Thermochemical decomposition of PAN increases exponentially with temperature and is more efficient at high NO/NO_2 ratios as PA reacts faster with NO than with NO_2 to reform PAN. Hence, the time scale of PAN towards thermochemical decomposition (τ_{chem}) is given by (Orlando et al., 1992; Shepson et al., 1992) as

$$\tau_{chem}(PAN) = \frac{1}{k_{1r}}\left(1 + \frac{k_{1f}[NO_2]}{k_2[NO]}\right) \quad (5)$$

In addition, loss of PA due to uptake by fog droplets can have an influence on the thermochemical decomposition of PAN (see Roberts et al., 1996; Villalta et al., 1996). However, since at night, when fog conditions may have occurred, the thermochemical decomposition of PAN was limited by the low temperatures, this effect was neglected for this study.

To evaluate whether PAN loss by thermochemical decomposition significantly impacted the MBR fluxes (Sect. 2.2), the chemical flux divergence between z_{ref} and z_0 due to thermochemical decomposition of PAN ($F_{chem_{surf}}$) was determined according to Doskey et al. (2004) by numeric integration of the thermochemical PAN loss as

$$F_{chem_{surf}} = \int_{z_0}^{z_{ref}} \frac{\rho_m(z) \cdot \chi_{PAN}(z)}{\tau_{chem}(z)}\, dz \quad (6)$$

The height dependent functions of $\chi_{PAN}(z)$ and $\tau_{chem}(z)$ were approximated by logarithmic interpolation between the available measurement heights of the required parameters and $\rho_m(z)$ was assumed to be constant with height (see Sect. 2.2).

The thermochemical PAN loss over the entire atmospheric boundary layer, represented as a flux ($F_{chem_{BL}}$), was obtained by integrating Eq. (6) from zero level to the height of the boundary layer (h_{BL})

$$F_{chem_{BL}} = \int_{0}^{h_{BL}} \frac{\rho_m(z) \cdot \chi_{PAN}(z)}{\tau_{chem}(z)}\, dz \quad (7)$$

Assuming a well-mixed boundary layer, the measured PAN concentration and NO/NO_2 ratio were taken as an average value for the whole boundary layer. As τ_{chem} is very sensitive to temperature, we assumed a dry adiabatic lapse rate of temperature with height. The height of

the nocturnal boundary layer was estimated from the nocturnal decline of O_3 and the corresponding measured $v_{D_{O_3}}$ from the relation given by (Shepson et al., 1992) (see also Sect. 3.3.3) as

$$h_{BL\_night} = 2 \cdot v_{D_{O_3}} \cdot ln \frac{\chi_{O_3}(t_0)}{\chi_{O_3}(t_1)} \quad (8)$$

where $\chi_{O_3}(t_0)$ and $\chi_{O_3}(t_1)$ are the O_3 mixing ratios at the start and end of the considered time interval, respectively. Since h_{BL_night} was determined from a boundary layer budget approach, it might not agree well with the real boundary layer height, as the nocturnal boundary layer might be significantly stratified. Instead, h_{BL_night} represents the theoretical depth of a mixed boundary layer, which was required in Eq. (7) to assume constant trace gas mixing ratios with height. The development of the diurnal boundary layer (h_{BL_day}) after dawn was modelled using the measured sensible heat surface flux and a simple encroachment approach implemented in the mixed layer model MXLCH (Vilà-Guerau de Arellano et al., 2011).

3 Results and discussions

3.1 Meteorological conditions: Classification of low and high NO_x episodes

The field experiment was dominated by wind directions from south west. These air masses were associated with relatively low levels of NO_x (= NO + NO_2) (ranging mainly between 1 and 10 ppb). Air masses from north easterly directions were much less frequent, but were often enriched with NO_x with values ranging mainly between 10 and 30 ppb (Fig. 1). This enrichment was mainly caused by advection from NO_x sources originated from the City of Mainz, nearby motor ways and other sources in the densely populated and industrialised Rhine-Main region. In contrast, the south west sector is dominated by farming without major industrial activity, thus representing an area with much less air pollution. Consequently, the occurrence of low and high NO_x situations during the field experiment was directly coupled to the wind direction and could be attributed to two contrasting synoptic conditions:

(1) Episodes under deep pressure influence and south westerly wind directions yielded low NO_x conditions. They were characterized by higher wind speeds, frequent cloud coverage, a mainly neutrally stratified boundary layer and typically lasted from 2 to 5 days.

(2) Sunny, convectively driven episodes with low wind speeds and, therefore, also varying wind directions resulted in high NO_x conditions, in cases when the wind direction was not from the south west sector. In contrast to the low NO_x conditions, these periods occurred sometimes as very isolated events and were associated with an unstable boundary layer during daytime and a stable stratification during nighttime.

For the further evaluation, entire days were selected and classified according to wind speed and wind direction. In total 20 days were classified as low NO_x and 27 days as high NO_x conditions. The diurnal averages of the meteorological conditions and micrometeorological characteristics during these days are displayed in Fig. 2a-f and mixing ratios of O_3, NO and NO_2 are shown in Fig. 2g-i. For both low and high NO_x, conditions photolysis of NO_2 contributed to the steady increase of NO mixing ratios after sunrise, which peaked between 8:00 and 10:00 CET and then declined with the growth of the daytime boundary layer. During high NO_x conditions both advection of freshly emitted NO from nearby sources and generally higher NO_2 levels lead to high NO mixing ratios exceeding sometimes 10 ppb. Biogenic NO emission from the grassland ecosystem, determined with the dynamic chamber method, were found to be insignificant (Plake et al., 2014). NO_2 mixing ratios showed a high variability during high NO_x conditions also indicating local sources. The daytime NO_2 decline was caused by both dilution due to the growing boundary layer and photolysis. It was anti-correlated with the increase of O_3 mixing ratios. The development of a shallow nocturnal inversion layer during high NO_x conditions caused increased O_3 removal rates. As a result, nighttime O_3 mixing ratios were lower than during low NO_x conditions. During daytime, both the higher insolation and the presence of pollutants under high NO_x conditions resulted in higher O_3 mixing ratios during the afternoon.

3.2 Characterisation of PAN under low and high NO_x conditions

The diurnal cycle of PAN mixing ratios was closely linked to the diurnal cycle of O_3. As for O_3, PAN mixing ratios increase after dawn to the maximum in the afternoon, with median values of 300 ppt under low and of 600 ppt under high NO_x conditions, respectively (Fig. 2j). The maximum is followed by a steady decrease over night to median values just before dawn of about 50 ppt under low NO_x and 200 ppt under high NO_x conditions.

The major reason for the much higher PAN levels during high NO_x conditions, are the elevated NO_2 mixing ratios, which occurred especially during nighttime and declined with the

onset of photolysis after dawn and the clearing of the nocturnal boundary layer. Comparing the diurnal evolution of PAN and O_3 mixing ratios, we find a higher PAN/O_3 ratio under high NO_x conditions at all times throughout the diurnal cycle. During peak PAN and O_3 mixing ratios in the afternoon, the PAN/O_3 ratio was 0.003 and 0.006 during low and high NO_x, conditions, respectively. Since photolytic production of O_3 from NO_2 was similar for both conditions, a large PAN/O_3 ratio implies a higher abundance of PA as a precursor of PAN (Zhang et al., 2009). Although no direct measurements of PA were available, the very low abundance of volatile organic compounds measured at the site (e.g., isoprene < 0.7 ppb, monoterpene < 0.3 ppb, J. Kesselmeier, personal communication, 2013) suggests that these higher levels of PA during high NO_x conditions primarily originated from anthropogenic non-methane hydrocarbons (NMHCs). Hence, PAN mixing ratios at the site were mainly influenced by advection from nearby pollution sources from north easterly directions.

The timescale for thermochemical decomposition of PAN, τ_{chem}, ranged for both low and high NO_x conditions mainly between 4 and 20 days at night (Fig. 2k). During daytime, τ_{PAN} ranged between 2 h and nearly one day (median ~5 h) for low NO_x conditions, but were significantly lower during high NO_x conditions (ranging between 30 min and 5 h; median ~2 h) caused by both on average higher NO/NO_2 ratios in the morning and higher temperatures in the afternoon.

3.3 Evaluation of PAN flux measurements

3.3.1 Deposition fluxes and canopy conductance

During the period of the PAN flux measurement mainly high NO_x conditions prevailed. The PAN fluxes showed a clear diurnal cycle with maximum deposition fluxes at midday and very small fluxes during nighttime (Fig. 3). Although the random flux errors were large compared to the observed fluxes (median ±0.035 nmol m^{-2} s^{-1}, see Moravek et al. (2014)) a daytime PAN deposition was clearly visible on most days. The gaps in the time series are due to extended instrument calibrations and maintenance of the GC-ECD. For the further evaluation PAN fluxes below the flux detection limit (34 % of data, see Sect. 2.2 for definition) were neglected, aside from data where $u_* < 0.07$ m s^{-1} (28 % of data) as this criterion would have eliminated most of the nighttime values.

The diurnal median values of the PAN and O_3 fluxes are shown in Fig. 4a-b. A diurnal course of the PAN flux is observed with maximal deposition fluxes of ~ -0.1 nmol m^{-2} s^{-1} during

daytime, which corresponds to $v_{D_{PAN}}$ at z_{ref} of ~ 0.3 cm s^{-1}. The visible short-term peaks are mostly attributed to the low number of data values ($\sum$n = 255) and also caused by the uncertainty of the MBR method. For O_3, this feature was much less pronounced due to the higher number of data points used ($\sum$n = 639). Both measured PAN fluxes and $v_{D_{PAN}}$ values were between the observations by Wolfe et al. (2009) (midday averages -0.04 nmol m^{-2} s^{-1}; $v_D \approx 0.1$ cm s^{-1}) and fluxes by Turnipseed et al. (2006) (midday averages ~-0.35 nmol m^{-2} s^{-1}; $v_D \approx 1$ cm s^{-1}) measured at two different pine forest sites in the USA during summer (Table 1). Daytime flux measurements at a grassland site by Doskey et al. (2004) resulted in an average $v_{D_{PAN}}$ of 0.13 cm s^{-1}. The magnitude of the daytime PAN flux at our site was about two orders of magnitude lower than the O_3 flux, yielding a median $v_{D_{PAN}} / v_{D_{O3}}$ ratio of 1.03. Comparison with experimentally derived PAN fluxes in the past (Table 1) reveals that $v_{D_{PAN}} / v_{D_{O3}}$ ratios vary considerably, which might be attributed to a large extent to the error of the applied measurement methods and the assumptions made. It has to be noted that v_D is height dependent, which can make its comparison between different studies difficult. However, the ratio $v_{D_{PAN}} / v_{D_{O3}}$ is largely independent from height in case the vertical profiles of PAN and O_3 concentrations are similar as it was shown at least for the data from our site.

The chemical flux divergence between z_{ref} and z_0 due to thermochemical decomposition of PAN (Eq. (6)) was found to be very small with the highest median value of 0.007 nmol m^{-2} s^{-1} at noon (Fig. 4a). In contrast, for the O_3 flux, the loss term due to reaction with NO and the production by NO_2 photolysis were significantly higher between 6:00 and 11:00 CET and led to a small net production of O_3 during daytime, which was corrected for in the presented fluxes.

The overall canopy conductance for PAN ($g_{c_{PAN}}$), representing the flux normalized by the concentration at z_0, shows a mean diurnal cycle with its maximum during daytime (Fig. 4c-d). The midday median values were around 0.4 cm s^{-1} and were similar to g_c values observed for O_3.

3.3.2 Stomatal uptake

During nighttime $g_{s_{PAN}}$ values were zero due to stomata closure (Fig. 4c). With the onset of radiation in the morning $g_{s_{PAN}}$ increases and reaches its maximum of 0.26 cm s^{-1} at

11:00 CET. As both $g_{s_{PAN}}$ and $g_{s_{O3}}$ differ only by the PAN and O_3 diffusivities (see Sect. 2.4), they show the same pattern, while $g_{s_{O3}}$ is larger by a factor of 1.6 due to the faster diffusivity of O_3. Due to an increased vapour pressure deficit in the afternoon the maximum values of $g_{s_{PAN}}$ and $g_{s_{O3}}$ are slightly skewed towards the morning.

The existence of a mesophyllic resistance limiting the stomatal uptake of PAN, as it was found by Teklemariam and Sparks (2004) or by (Sparks et al., 2003) at high stomatal conductance, cannot be validated from our data. Only if the modelled $g_{s_{PAN}}$ values exceeded the experimentally determined $g_{c_{PAN}}$ values, a limitation could be suspected. It is suggested that the mesophyllic uptake of PAN is lower than for O_3, as there are less reaction sites for PAN within the plant cell and its reaction with proteins is slower, although the mesophyll biochemistry for PAN assimilation is not clearly understood (Doskey et al., 2004).

3.3.3 Non-stomatal deposition

According to the MBR flux measurements at our site, the non-stomatal sink played a major role with median midday $g_{ns_{PAN}}$ values ranging between 0.05 and 0.4 cm s^{-1}, corresponding to a non-stomatal resistance ($R_{ns} = g_{ns}^{-1}$) of 2000 and 240 s m^{-1}, respectively. The nighttime $g_{ns_{PAN}}$ values are very low, but have to be treated with caution due to the uncertainties of the MBR method at night. The peaks in $g_{ns_{PAN}}$ are mainly associated with the uncertainties of $g_{c_{PAN}}$ caused by the limited amount of data (see Sect. 3.3.1). For O_3, we observed a clear diurnal cycle with lowest values in the afternoon. The diurnal cycle could be well reproduced as a function of relative humidity multiplied by LAI, despite elevated values between 06:00 and 10:00 CET, where surface humidity is still very high and the NO_x advection might lead to a greater uncertainty of the chemical production and loss of terms (Sect. 3.3.1).

Since uncertainties in the O_3 flux impact the PAN flux directly, we discarded data with large NO_x values for the evaluation of $g_{ns_{PAN}}$ as well as values where $u_* < 0.07$ m s^{-1}. We could not identify any significant dependency of the individual data points of g_{ns} on temperature, relative humidity or surface wetness. This contradicts the assumption of Shepson et al. (1992), who suspected that $g_{ns_{PAN}}$ would decrease with higher surface wetness due to the low deposition on water surfaces (Kames et al., 1991). Turnipseed et al. (2006) explained a maximum of $v_{D_{PAN}}$ after sunrise with increased deposition to leaf surface water of a pine forest canopy and hypothesize the existence of a reactive uptake process within the leaf water.

However, our findings support the results by Schrimpf et al. (1996), who did not observe a relationship of $g_{ns_{PAN}}$ with relative humidity.

For the determination of $F_{model_{PAN}}$ over the entire measurement period (see Sect. 2.4) an estimate or parameterisations of $g_{ns_{PAN}}$ is required. Since from our data, no significant dependency was found and nighttime values are uncertain, we assume a constant value of $g_{ns_{PAN}}$. Hence, we derived a bulk $g_{ns_{PAN}}$ value by correlating the measured PAN fluxes with a modelled PAN flux using a series of different $g_{ns_{PAN}}$ values in Eq. (2). The smallest root mean square error was obtained with an optimal g_{ns} value of 0.28 cm s^{-1} for the whole dataset, which corresponds to $R_{ns_{PAN}}$ = 360 s m^{-1}. This resistance value is in the range of findings by other studies, e.g., Turnipseed et al. (2006) observed a median value of 244 s m^{-1} under dry and 125 s m^{-1} under wet conditions.

To obtain another independent estimate of the non-stomatal deposition, we employed the nocturnal boundary layer budget (NBLB) method according to Shepson et al. (1992), which compares the nocturnal PAN decay to that of O_3 and yields a ratio of PAN to O_3 deposition velocities. The main assumption, that the decline of both PAN and O_3 mixing ratio during nighttime was only due to deposition, is valid as chemical reactions are negligible at night for both PAN (see Fig. 2l) and O_3 (no photolysis and low NO mixing ratios). We analysed in total 16 nights, where a clear logarithmic decline of both PAN and O_3 mixing ratios was observed and where the main wind direction was within the "clean" sector in the south west. Using only nights with a good correlation between both PAN and O_3 decline ($R^2 > 0.7$), we obtain an average value for $v_{D_{PAN}}/v_{D_{O3}}$ of 1.75, which is similar to the average value obtained by Shepson et al. (1992). As stomatal uptake is assumed to be zero at night, we obtained according to Eq. (3) a bulk $g_{ns_{PAN}}$ of 0.5 cm s^{-1} ($R_{ns_{PAN}}$ = 200 s m^{-1}). This value of $g_{ns_{PAN}}$ is slightly larger than the value obtained from the MBR measurement.

In currently applied deposition models (e.g., Simpson et al., 2012), $g_{ns_{PAN}}$ is often derived according to Wesely (1989) as a composite between the non-stomatal conductance of sulphur dioxide ($g_{ns_{SO2}}$) and $g_{ns_{O3}}$

$$g_{ns_{PAN}} = 10^{-5} \cdot H^*_{PAN} \cdot g_{ns_{SO2}} + f_{0_{PAN}} \cdot g_{ns_{O3}} \quad (9)$$

SO_2 represents a very soluble substance (effective Henry constant $H^*_{SO_2}$ = 10^5 M atm^{-1}) and O_3 a compound that reacts fast with substances in the leaf cuticles such as protein thiols (Mudd,

1982). Due to the poor solubility of PAN in water (H^*_{PAN} = 4.1 M atm^{-1}, see Kames and Schurath (1995)) the first term of the right side of Eq. (9) can be neglected and only the reactivity index, f_0, is of significant importance. According to Wesely (1989) $f_{0_{PAN}}$ = 0.1, which suggests the non-stomatal deposition of PAN would be about one order of magnitude lower than for O_3. Zhang et al. (2002) suggest a $f_{0_{PAN}}$ = 0.6 based on first studies on PAN deposition by Hill (1971) and Garland (1977). This contradicts our findings by both the MBR and the NBLB method, which observed at least equal or even higher non-stomatal deposition for PAN than for O_3, and supports the statement by Turnipseed et al. (2006) that current deposition models may significantly underestimate PAN non-stomatal deposition.

3.4 PAN deposition fluxes for low and high NO_x conditions

To evaluate the PAN deposition under both low and high NO_x conditions as well as its potential influence on the natural grassland ecosystem and its role for the atmospheric N_r budget, the PAN deposition flux was modelled for the entire period from 29 June to 21 October (see Sect. 2.4). For this, we used the bulk value for $g_{ns_{PAN}}$ of 0.28 cm s^{-1} (Sect. 3.3.3) for both low and high NO_x, as we found this to be the best estimate from our data. The obtained median diurnal cycles of $F_{model_{PAN}}$ for low and high NO_x conditions (Fig. 5) reveal that the total deposition (i.e. stomatal + non-stomatal) was more than twice as high during high NO_x (~-0.1 nmol m^{-2} s^{-1}) than during low NO_x (~-0.05 nmol m^{-2} s^{-1}) conditions, which is mainly attributed to the higher PAN mixing ratios during high NO_x conditions. Median midday deposition velocities were very similar during both episodes ($v_{D_{PAN}} \approx$ 0.5 cm s^{-1}). As already discussed in Sect. 3.3.3, the non-stomatal pathway was significant, which is reflected by a daytime fraction of $g_{ns_{PAN}}/g_{c_{PAN}}$ of 0.7 during low NO_x and 0.6 during high NO_x conditions. As about half of the grassland vegetation was senescing or was already dead, reaction on plant surfaces may be a reason for the large non-stomatal fraction.

The importance of PAN deposition as a loss process of PAN from the atmosphere is determined by comparison to the magnitude of the thermochemical decomposition of PAN in the boundary layer (Eq. (7)). Due to the lower temperatures and the lack of NO at night, the nocturnal thermochemical loss was insignificant during both low and high NO_x conditions. Using the boundary layer budget approach (Eq. (8)), we found h_{BL_night} to be on average 200 m (Fig. 5). In contrast, during daytime the thermochemical loss constituted the largest

PAN sink, during both low and high NO_x conditions. After dawn, h_{BL_day} grew during high NO_x conditions on average up to 1200 m, whereas its development was slightly suppressed during low NO_x conditions. The modelled boundary layer height was compared for selected days to the boundary layer height obtained from a WRF model. The WRF model yielded slightly higher daytime maximum values ranging from 1100 up to 1700 m. When the boundary was well mixed (11-17 CET), the thermochemical loss during high NO_x conditions was about 3.5 times higher than during low NO_x conditions. This was caused by a combination of (a) the higher PAN mixing ratios (effect: 59 %), (b) the reduced reaction time scale due to higher temperatures and larger NO to NO_2 ratios (effect: 34 %) and to some extend also by (c) the higher boundary layer (effect: 7 %). A summary of the relevant parameters for nighttime and daytime conditions is given in Table 2, where the timescales for PAN deposition is given by $\tau_{dep} = \rho_m \cdot \chi_{PAN} \cdot F^{-1}_{model_{PAN}} \cdot h_{BL}$ The reaction rates towards PAN deposition (k_{dep}) and thermochemical decomposition over the entire boundary layer height ($k_{chem_{BL}}$) are the inverse values of τ_{dep} and $\tau_{chem_{BL}}$, respectively.

Integrating $F_{model_{PAN}}$ and $F_{chem_{BL}}$ over the entire diel cycle yields the total mass of PAN removed per unit area by dry deposition (L_{dep}) and thermochemical decomposition ($L_{chem_{BL}}$), respectively (McFadyen and Cape, 1999; Turnipseed et al., 2006). As presented in Table 2, during low NO_x conditions dry deposition made up 32 %, whereas under high NO_x conditions it contributed with 22 %. to the diurnal PAN removal within the boundary layer. These values are slightly lower as the ones given by McFadyen and Cape (1999), who suggest equal PAN loss via both processes. Although they claim very low NO/NO_2 ratios at the site to be a major reason for the low chemical loss, an overestimation of the PAN deposition in their study is possible, since it was not measured directly. Accounting for a temperature decrease with height, Turnipseed et al. (2006) estimated a maximal contribution of dry deposition of 10%. Wolfe et al. (2009) found that dry deposition accounted only for 3% of the total PAN loss during warm and 13% during cool periods.

To evaluate its significance as a source of N_r to the grassland ecosystem, PAN deposition has to be evaluated in relation to other N_r sources. Dennis et al. (2013) estimate a contribution of dry deposition of PANs (i.e. the sum of all PAN species) of about 3.5% to the total dry and wet nitrogen annual deposition in the continental USA. However, their values are based on the parameterisation by Zhang et al. (2002), which might significantly underestimate dry deposition of PAN as found e.g. by Turnipseed et al. (2006) and in this study. Stevens et al.

(2010) evaluated the effect of total inorganic nitrogen deposition on grasslands across Europe and found that species richness decreased with sites that were subject to higher nitrogen deposition. The observed PAN removal via dry deposition (i.e., L_{dep}) over one entire day was in this study 333 µg m^{-2} d^{-1} during low and 518 µg m^{-2} d^{-1} during high NO_x conditions (Table 2). This is much lower than the total nitrogen deposition observed at the sites reported by Stevens et al. (2010) ranging between 4.7 and 104.2 mg m^{-2} d^{-1} (equivalent to 2 and 44 kg N ha^{-1} a^{-1}), which suggests that PAN deposition under both low and high NO_x does not play a critical role on plant species richness at our site. Moreover, PAN mixing ratios observed at our site were significantly below the threshold given for phytotoxic effect on plants (between 15 and 25 ppb, see Temple and Taylor, 1983).

4 Conclusions

Up to date very few studies have directly measured PAN deposition to ecosystems. Previous experiments often cover only a short time period and obtained results differ considerably. In particular, the relationship between PAN and O_3 deposition has remained inconclusive. Based on the MBR method, we find a considerable non-stomatal uptake of PAN ($g_{ns_{PAN}}$ = 0.28 cm s^{-1}). This resulted in an equal or even higher non-stomatal conductance for PAN than for O_3, most likely suggesting an underestimation of PAN deposition by current models. We did not find a relation of the non-stomatal conductance for PAN with other quantities, such as relative humidity. However, it cannot be fully excluded that this may also be attributed to the limited PAN flux data above the flux detection limit. The modelled stomatal uptake did not exceed the overall deposition, suggesting that stomatal uptake is not limited by further, not-considered resistances.

PAN deposition at our measurement site was governed by two contrasting pollution regimes, (1) low NO_x episodes with clean air from south westerly directions and (2) high NO_x episodes with more polluted air masses from the north eastern sector. Under high NO_x conditions, locally produced PAN from the industrialized region was advected to the site, leading to PAN mixing ratios which were a factor of two to four higher than under low NO_x conditions. Hence, PAN deposition during these episodes was larger with daytime maxima of -0.1 nmol m^{-2} s^{-1}. However, as also found in previous studies, the largest fraction of PAN loss during daytime was due to thermochemical decomposition of PAN. For clean conditions dry deposition accounted for about 32 % of the daytime PAN loss, while it only accounted for

22 % during polluted conditions. The higher thermochemical PAN loss during polluted episodes was mainly associated with different meteorological conditions and only to some extend caused by larger NO/NO_2 ratios, due to freshly emitted NO by nearby sources. During nighttime non-stomatal PAN deposition was the only significant PAN sink.

A comparison of PAN deposition at the site with other deposition pathways of atmospheric reactive nitrogen suggests that PAN deposition only played a minor role as a potential nitrogen source to the nutrient-poor natural grassland ecosystems in this study. However, up to date still little is known about the direct uptake of PAN by vegetation and the effect on their metabolism. Furthermore, studies which performed direct PAN flux measurements are limited to only a few types of ecosystems and conditions, and are often prone to large uncertainties. As suggested by other studies in the past, PAN deposition might be the dominant removal process of atmospheric PAN in winter at lower temperatures. However, up to date in situ PAN flux measurements only cover late spring to early autumn periods in the northern hemisphere. Hence, both in situ flux measurements of PAN during different seasons and for a larger variety of ecosystems, as well as detailed studies on the role of non-stomatal uptake mechanisms to improve current deposition models are desirable tasks for future research on PAN deposition.

Acknowledgements

This project was funded by the Max Planck Society. J.-C. Mayer and D. Plake contributed to the setup and operation of additional measurements at the field site. L. Smoydzin applied the WRF model for the estimation of the boundary layer height. We thank C. Ammann and D. Plake for discussion on the flux divergence and chemical correction methods.

References

Brown, S.S., Stutz, J., 2012. Nighttime radical observations and chemistry. Chemical Society Reviews 41, 6405-6447.

Businger, J.A., 1986. Evaluation of the Accuracy with Which Dry Deposition Can Be Measured with Current Micrometeorological Techniques. J Clim Appl Meteorol 25, 1100-1124.

Cazorla, M., Brune, W.H., 2010. Measurement of Ozone Production Sensor. Atmos. Meas. Tech. 3, 545-555.

De Bruin, H.A.R., Moore, C.J., 1985. Zero-Plane Displacement and Roughness Length for Tall Vegetation, Derived from a Simple Mass Conservation Hypothesis. Boundary-Layer Meteorology 31, 39-49.

Dennis, R.L., Schwede, D.B., Bash, J.O., Pleim, J.E., Walker, J.T., Foley, K.M., 2013. Sensitivity of continental United States atmospheric budgets of oxidized and reduced nitrogen to dry deposition parametrizations. Philos T R Soc B 368, 20130124.

Doskey, P.V., Kotamarthi, V.R., Fukui, Y., Cook, D.R., Breitbeil, F.W., Wesely, M.L., 2004. Air-surface exchange of peroxyacetyl nitrate at a grassland site. J. Geophys. Res.-Atmos. 109, 9, D10310.

EUROSTAT, 2011. Agricuture and fishery statistics: main results 2009-10, 2011 ed. Publications Office of the European Union, Luxembourg, p. 152.

Foken, T., Leuning, R., Oncley, S., Mauder, M., Aubinet, M., 2012. Corrections and Data Quality Control, in: Aubinet, M., Vesala, T., Papale, D. (Eds.), Eddy Covariance. Springer Netherlands, pp. 85-131.

Foken, T., Wichura, B., 1996. Tools for quality assessment of surface-based flux measurements. Agr Forest Meteorol 78, 83-105.

Garland, J.A., 1977. The dry deposition of sulphur dioxide to land and water surfaces. Proc. R. Soc. London Ser. A-Math. Phys. Eng. Sci. 354, 245-268.

Garland, J.A., Penkett, S.A., 1976. Absorption of peroxy acetyl nitrate and ozone by natural surfaces. Atmos. Environ. 10, 1127-1131.

Hicks, B.B., Baldocchi, D.D., Meyers, T.P., Hosker, R.P., Matt, D.R., 1987. A preliminary multiple resistance routine for deriving dry deposition velocities from measured quantities. Water Air Soil Poll 36, 311-330.

Hill, A.C., 1971. Vegetation - sink for atmospheric pollutants. Journal of the Air Pollution Control Association 21, 341-346.

Kames, J., Schurath, U., 1995. Henrys Law and Hydrolysis-Rate Constants for Peroxyacyl Nitrates (Pans) Using a Homogeneous Gas-Phase Source. J. Atmos. Chem. 21, 151-164.

Kames, J., Schweighoefer, S., Schurath, U., 1991. Henrys Law Constant and Hydrolysis of Peroxyacetyl Nitrate (Pan). J. Atmos. Chem. 12, 169-180.

Lamaud, E., Loubet, B., Irvine, M., Stella, P., Personne, E., Cellier, P., 2009. Partitioning of ozone deposition over a developed maize crop between stomatal and non-stomatal uptakes, using eddy-covariance flux measurements and modelling. Agr Forest Meteorol 149, 1385-1396.

Liu, H.P., Foken, T., 2001. A modified Bowen ratio method to determine sensible and latent heat fluxes. Meteorol. Z. 10, 71-80.

Mauder, M., Foken, T., 2011. Documentation and Instruction Manual of the Eddy-Covariance Software Package TK3, Arbeitsergebnisse. Abteilung Mikrometeorologie, Universität Bayreuth, Bayreuth, pp. 60, ISSN 1614-8916.

McFadyen, G.G., Cape, J.N., 1999. Physical and chemical influences on PAN concentrations at a rural site. Atmos. Environ. 33, 2929-2940.

Moravek, A., Foken, T., Trebs, I., 2014. Application of a GC-ECD for measurements of biosphere–atmosphere exchange fluxes of peroxyacetyl nitrate using the relaxed eddy accumulation and gradient method. Atmos. Meas. Tech. 7, 2097-2119.

Moravek, A., Trebs, I., Foken, T., 2013. Effect of imprecise lag time and high-frequency attenuation on surface-atmosphere exchange fluxes determined with the relaxed eddy accumulation method. Journal of Geophysical Research: Atmospheres 118, 10210-10224.

Mudd, J.B., 1982. Effects of oxidants on metabolic function, in: Unsworth, M.H., Ormrod, D.P. (Eds.), Effects of Gaseous Air Pollution in Agriculture and Horticulture. Butterworth-Heinemann, Woburn, Mass., pp. 189–203.

Okano, K., Tobe, K., Furukawa, A., 1990. Foliar Uptake of Peroxyacetyl Nitrate (PAN) by Herbaceous Species Varying in Susceptibility to this Pollutant. New Phytol 114, 139-145.

Orlando, J.J., Tyndall, G.S., Calvert, J.G., 1992. Thermal-Decomposition Pathways for Peroxyacetyl Nitrate (Pan) - Implications for Atmospheric Methyl Nitrate Levels. Atmos Environ a-Gen 26, 3111-3118.

Oswald, R., Behrendt, T., Ermel, M., Wu, D., Su, H., Cheng, Y., Breuninger, C., Moravek, A., Mougin, E., Delon, C., Loubet, B., Pommerening-Roser, A., Sorgel, M., Poschl, U., Hoffmann, T., Andreae, M.O., Meixner, F.X., Trebs, I., 2013. HONO Emissions from Soil Bacteria as a Major Source of Atmospheric Reactive Nitrogen. Science 341, 1233-1235.

Plake, D., Stella, P., Moravek, A., Mayer, J.-C., Ammann, C., Held, A., Trebs, I., 2014. Comparison of ozone fluxes measured with the dynamic chamber and the eddy covariance method and partitioning between stomatal and non stomatal deposition. Agricultural and Forest Meteorology (in review).

Rannik, U., Aubinet, M., Kurbanmuradov, O., Sabelfeld, K.K., Markkanen, T., Vesala, T., 2000. Footprint analysis for measurements over a heterogeneous forest. Boundary-Layer Meteorology 97, 137-166.

Roberts, J.M., Parrish, D.D., Norton, R.B., Bertman, S.B., Holloway, J.S., Trainer, M., Fehsenfeld, F.C., Carroll, M.A., Albercook, G.M., Wang, T., Forbes, G., 1996. Episodic removal of NOy species from the marine boundary layer over the North Atlantic. Journal of Geophysical Research: Atmospheres 101, 28947-28960.

Rummel, U., Ammann, C., Kirkman, G.A., Moura, M.A.L., Foken, T., Andreae, M.O., Meixner, F.X., 2007. Seasonal variation of ozone deposition to a tropical rain forest in southwest Amazonia. Atmos. Chem. Phys. 7, 5415-5435.

Schrimpf, W., Lienaerts, K., Muller, K.P., Rudolph, J., Neubert, R., Schussler, W., Levin, I., 1996. Dry deposition of peroxyacetyl nitrate (PAN): Determination of its deposition velocity at night from measurements of the atmospheric PAN and (222)Radon concentration gradient. Geophys. Res. Lett. 23, 3599-3602.

Shepson, P.B., Bottenheim, J.W., Hastie, D.R., Venkatram, A., 1992. Determination of the relative ozone and PAN deposition velocities at night. Geophys. Res. Lett. 19, 1121-1124.

Simpson, D., Benedictow, A., Berge, H., Bergstrom, R., Emberson, L.D., Fagerli, H., Flechard, C.R., Hayman, G.D., Gauss, M., Jonson, J.E., Jenkin, M.E., Nyiri, A., Richter, C., Semeena, V.S., Tsyro, S., Tuovinen, J.P., Valdebenito, A., Wind, P., 2012. The EMEP MSC-W chemical transport model - technical description. Atmos. Chem. Phys. 12, 7825-7865.

Singh, H.B., 1987. Reactive Nitrogen in the Troposphere. Environ Sci Technol 21, 320-327.

Sparks, J.P., Roberts, J.M., Monson, R.K., 2003. The uptake of gaseous organic nitrogen by leaves: A significant global nitrogen transfer process. Geophys. Res. Lett. 30.

Stella, P., Personne, E., Loubet, B., Lamaud, E., Ceschia, E., Beziat, P., Bonnefond, J.M., Irvine, M., Keravec, P., Mascher, N., Cellier, P., 2011. Predicting and partitioning ozone fluxes to maize crops from sowing to harvest: the Surfatm-O-3 model. Biogeosciences 8, 2869-2886.

Stevens, C.J., Duprè, C., Dorland, E., Gaudnik, C., Gowing, D.J.G., Bleeker, A., Diekmann, M., Alard, D., Bobbink, R., Fowler, D., Corcket, E., Mountford, J.O., Vandvik, V., Aarrestad, P.A., Muller, S., Dise, N.B., 2010. Nitrogen deposition threatens species richness of grasslands across Europe. Environ Pollut 158, 2940-2945.

Suttie, J.M., Reynolds, S.G., Batello, C., 2005. Grasslands of the world. FAO, Rome.

Talukdar, R.K., Burkholder, J.B., Schmoltner, A.M., Roberts, J.M., Wilson, R.R., Ravishankara, A.R., 1995. Investigation of the Loss Processes for Peroxyacetyl Nitrate in the Atmosphere - Uv Photolysis and Reaction with Oh. J. Geophys. Res.-Atmos. 100, 14163-14173.

Teklemariam, T.A., Sparks, J.P., 2004. Gaseous fluxes of peroxyacetyl nitrate (PAN) into plant leaves. Plant Cell Environ. 27, 1149-1158.

Temple, P.J., Taylor, O.C., 1983. World-wide ambient measurements of peroxyacetyl nitrate (PAN) and implications for plant injury. Atmospheric Environment (1967) 17, 1583-1587.

Turnipseed, A.A., Huey, L.G., Nemitz, E., Stickel, R., Higgs, J., Tanner, D.J., Slusher, D.L., Sparks, J.P., Flocke, F., Guenther, A., 2006. Eddy covariance fluxes of peroxyacetyl nitrates (PANs) and NOy to a coniferous forest. J. Geophys. Res.-Atmos. 111, D09304.

Vilà-Guerau de Arellano, J., Patton, E.G., Karl, T., van den Dries, K., Barth, M.C., Orlando, J.J., 2011. The role of boundary layer dynamics on the diurnal evolution of isoprene and the hydroxyl radical over tropical forests. Journal of Geophysical Research: Atmospheres 116, D07304.

Villalta, P.W., Lovejoy, E.R., Hanson, D.R., 1996. Reaction probability of peroxyacetyl radical on aqueous surfaces. Geophys. Res. Lett. 23, 1765-1768.

Wesely, M.L., 1989. Parameterization of surface resistances to gaseous dry deposition in regional-scale numerical-models. Atmos. Environ. 23, 1293-1304.

Wesely, M.L., Hicks, B.B., 2000. A review of the current status of knowledge on dry deposition. Atmos. Environ. 34, 2261-2282.

Wolfe, G.M., Thornton, J.A., Yatavelli, R.L.N., McKay, M., Goldstein, A.H., LaFranchi, B., Min, K.E., Cohen, R.C., 2009. Eddy covariance fluxes of acyl peroxy nitrates (PAN, PPN and MPAN) above a Ponderosa pine forest. Atmos. Chem. Phys. 9, 615-634.

Zhang, J.M., Wang, T., Ding, A.J., Zhou, X.H., Xue, L.K., Poon, C.N., Wu, W.S., Gao, J., Zuo, H.C., Chen, J.M., Zhang, X.C., Fan, S.J., 2009. Continuous measurement of peroxyacetyl nitrate (PAN) in suburban and remote areas of western China. Atmos. Environ. 43, 228-237.

Zhang, L., Moran, M.D., Makar, P.A., Brook, J.R., Gong, S., 2002. Modelling gaseous dry deposition in AURAMS: a unified regional air-quality modelling system. Atmos. Environ. 36, 537-560.

Tables and Figures

Table 1. Comparison of PAN fluxes and deposition velocities at the Mainz-Finthen grassland with previous studies. All field experiments were performed in the mid-latitudes of the northern hemisphere within the period of late spring to early autumn.

Method	Vegetation /location	LAI (one sided	Flux (nmol m^{-2} s^{-1}) day	night	v_D (cm s^{-1}) day	night	$v_{D_{PAN}}/v_{D_{O_3}}$ (–) day	night	Study
EC (CIMS)	pine forest	3.5	-0.35	-0.05	~0.7	~0.3	–	> 1	Turnipseed et al. (2006)
	pine forest	5.1	-0.04	-0.03	0.30	0.10	1.25	0.5	Wolfe et al. (2009)†
Gradient /MBR	corn field	–	–	–	–	0.54	–	–	Schrimpf et al. (1996)
	grassland	–	–	–	0.13	–	0.2- 0.3	–	Doskey et al. (2004) ‡
	grassland	4.8	-0.07	-0.01	0.30	0.06	1.03	1.25	this study
NBLB	n.s.	–	–	–	–	–	–	0.31	Garland and Penkett (1976) ‡
	forest, agric.	–	–	–	–	–	–	2.38	Shepson et al. (1992) ‡
	rural, sea-side	–	–	–	–	–	–	1.1 – 6.2	McFadyen and Cape (1999) ‡
	grassland	4.8	–	–	–	–	–	1.75	this study (see Sect. 3.3.3)
Laboratory	alfalfa	–	–		–		0.37		Hill (1971)
	grass	–	–		0.25		0.5		Garland and Penkett (1976)
	trees, crops	–	-0.02 – -0.06		0.00 – 1.50		–		Sparks et al. (2003)
	trees, herb.	–	-0.01 – -0.02		0.11 – 0.34		–		Teklemariam and Sparks

† net flux; in-canopy production of PAN was observed
‡ O_3 flux not was not measured directly

Table 2. Modelled PAN deposition and thermochemical loss for low and high NO_x conditions at the Mainz-Finthen grassland site. The description of the shown parameters is given in the text.

	PAN (ppt)	T (°C)	NO/NO_2 (-)	h_{BL} (m)	τ_{dep} (d)	$\tau_{chem_{BL}}$ (d)	k_{dep} (s^{-1})	$k_{chem_{BL}}$ (s^{-1})	L_{dep} (µg m^{-2} d^{-1})	$L_{chem_{BL}}$ (µg m^{-2} d^{-1})	L_{dep} (%)
Low NO_x											
daytime	182	17.6	0.18	567	1.50	0.88	$1.8 \cdot 10^{-4}$	$3.2 \cdot 10^{-4}$			
nighttime	147	13.6	0.01	200	0.42	16.08	$6.7 \cdot 10^{-4}$	$0.17 \cdot 10^{-4}$			
all									333	698	32
High NO_x											
daytime	405	20	0.23	641	1.54	0.54	$1.8 \cdot 10^{-4}$	$5.1 \cdot 10^{-4}$			
nighttime	334	15.9	0.01	200	0.83	12.67	$3.3 \cdot 10^{-4}$	$0.21 \cdot 10^{-4}$			
all									518	1840	22

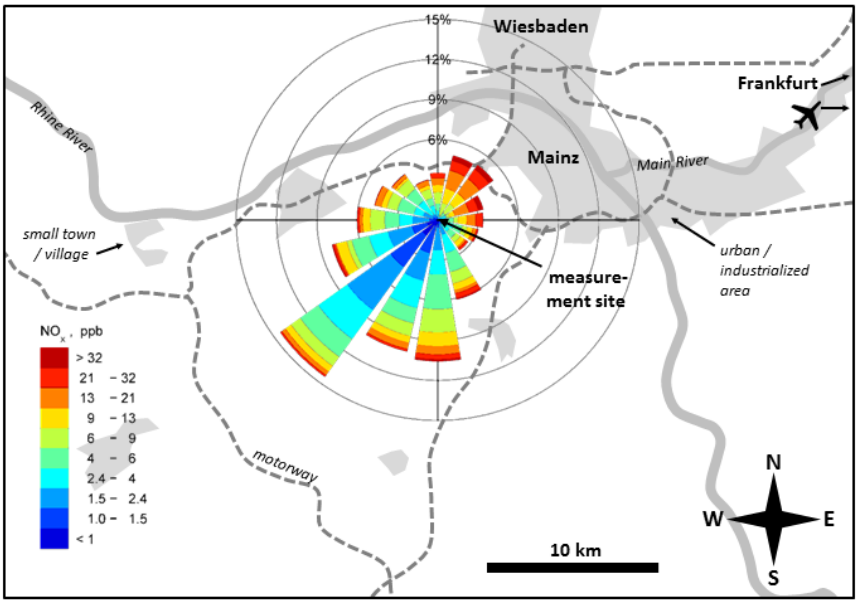

Fig. 1. Location of the Mainz-Finthen grassland site located at the edge of the industrialized Rhine-Main-Area in Germany. The wind rose, centred at the measurement site, indicates unpolluted (low NO_x) air masses from the south west sector and more polluted (high NO_x) air masses from north easterly directions.

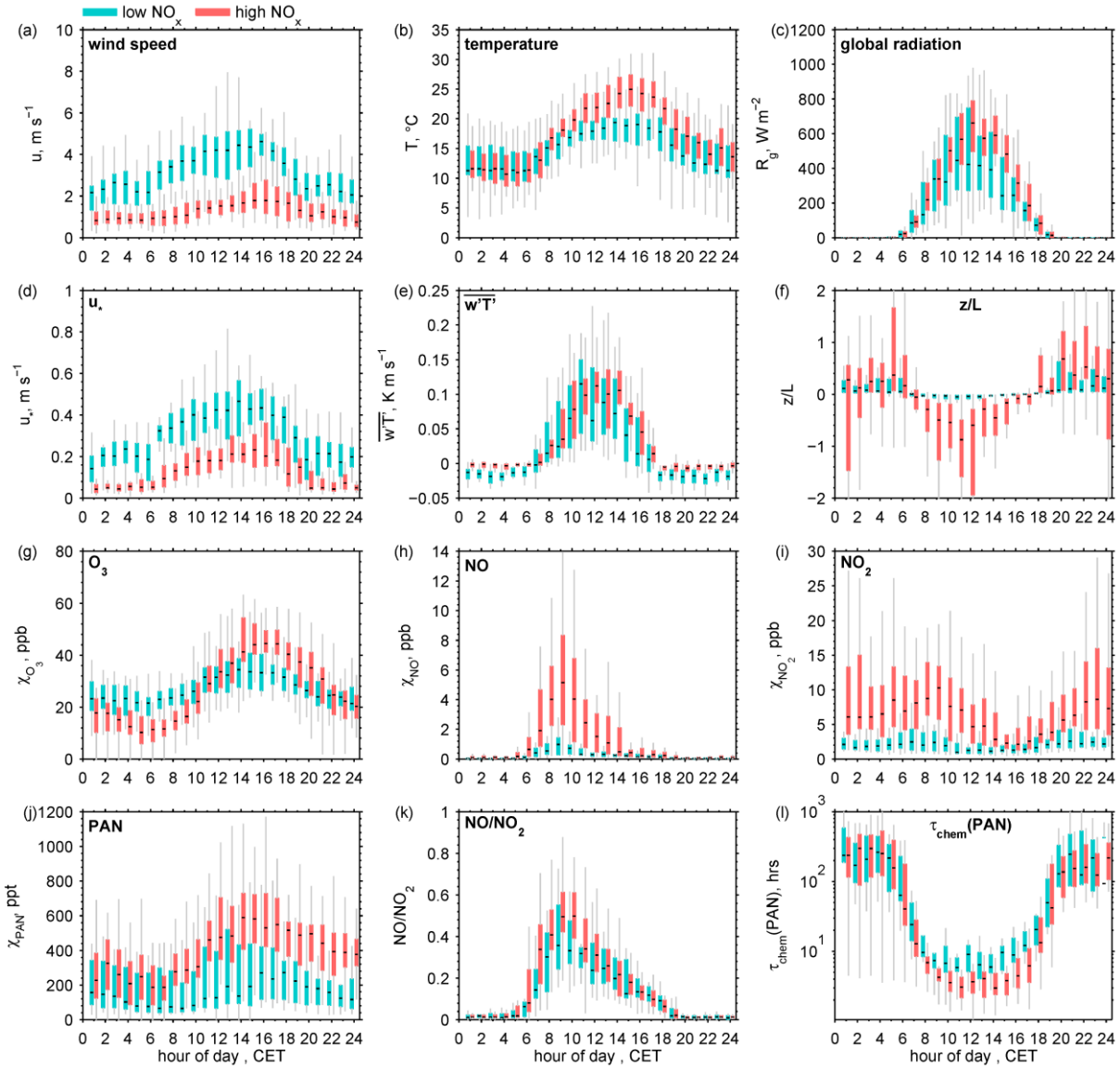

Fig. 2. Diurnal boxplot statistics for the period from 29 June to 21 October 2011 at the Mainz-Finthen grassland site, characterising low and high NO_x periods according to the prevailing meteorological conditions (a-f), mixing ratios of the O_3-NO-NO_2 triad (g-i) and PAN mixing ratios including the NO/NO_2 ratio used for the calculation of τ_{chem} (j-l).

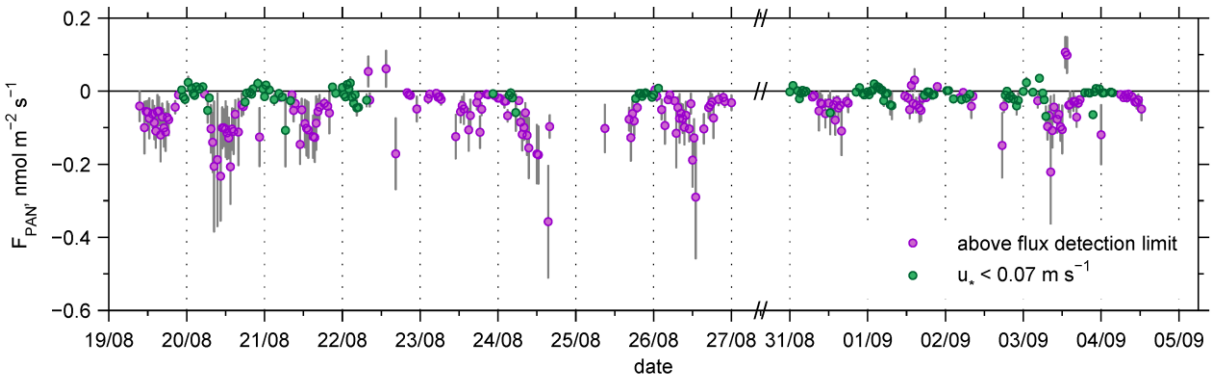

Fig. 3. Overview of PAN flux measurements using the MBR method from 19 August to 4 September 2011 at the Mainz-Finthen grassland site after applying quality criteria as described in Moravek et al. (2014). Error bars represent the random flux error and green values indicate periods with weak turbulent exchange ($u_* < 0.07$ m s^{-1}).

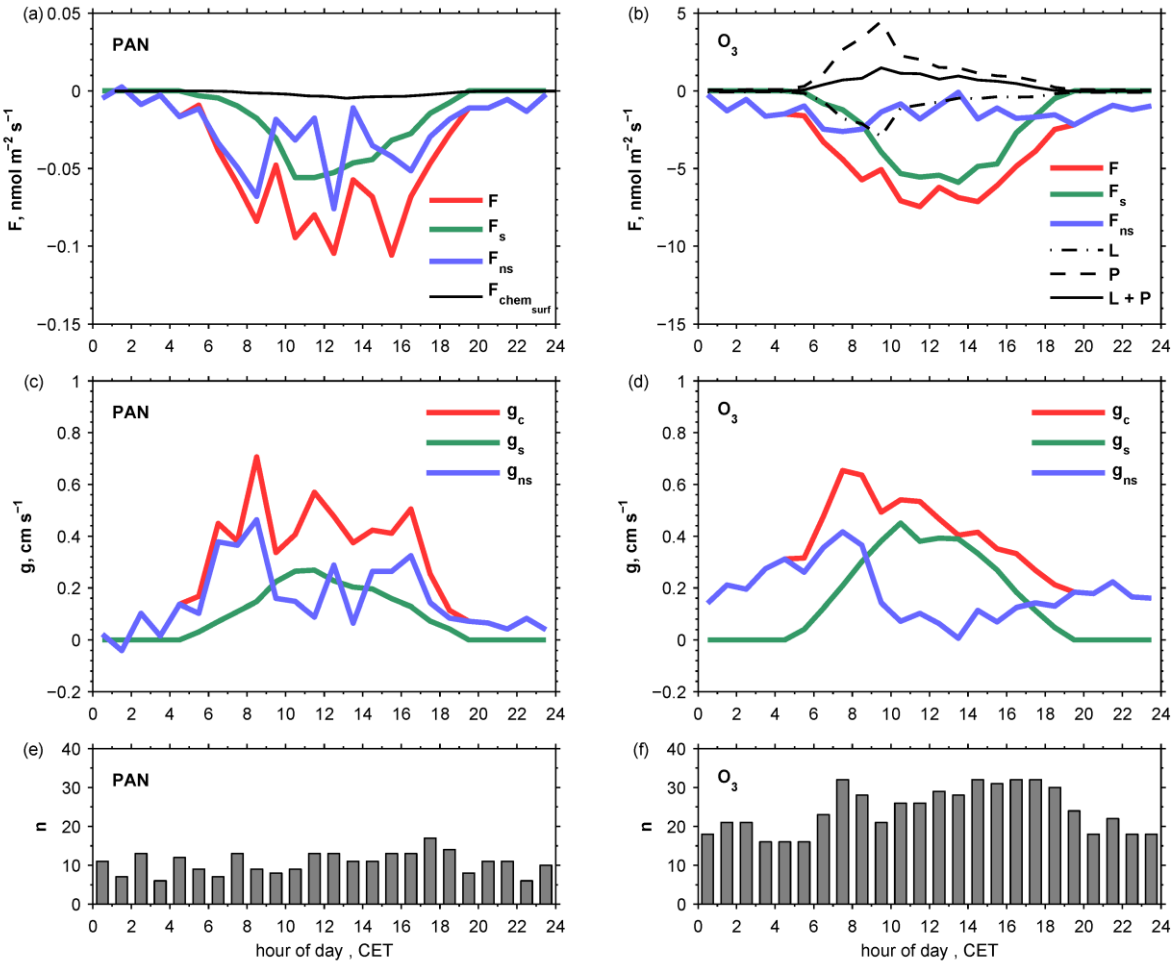

Fig. 4. Flux partitioning of PAN (left column) and O_3 (right column) deposition into stomatal and non-stomatal pathways at the Mainz-Finthen grassland site. Shown are diurnal median values for the period from 19 August to 4 September 2011. Panels (a) and (b) indicate the deposition fluxes inlcuding the thermochemical flux term ($F_{chem_{surf}}$) for PAN and the loss (L) and production (P) terms for O_3. Panels (c) and (d) show the resepective conductances, while (e) and (f) show the number data points used for every hourly interval.

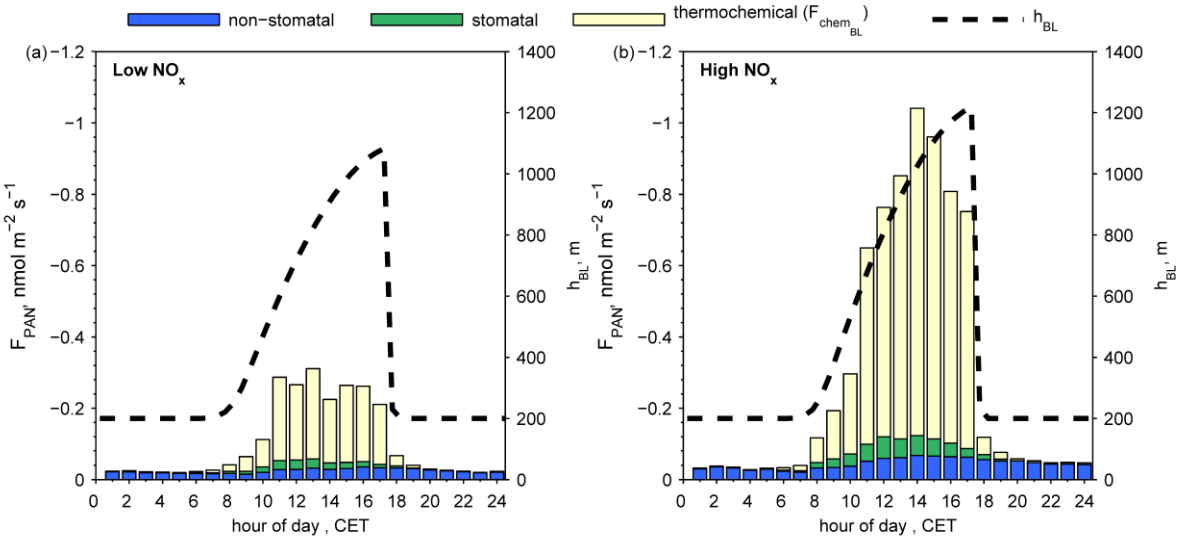

Fig. 5. Modelled stomatal and non-stomatal PAN deposition fluxes and PAN loss due to thermochemical decomposition for (a) low and (b) high NO_x periods at the Mainz-Finthen grassland site. The dashed line marks the theoretical boundary layer height used for the calculation of the PAN decomposition (for details see text).